ELSEVIER

PII S0730-725X(98)00107-6

● *Original Contribution*

WATER SIGNAL ATTENUATION IN DIFFUSION-WEIGHTED ¹H NMR EXPERIMENTS DURING CEREBRAL ISCHEMIA: INFLUENCE OF INTRACELLULAR RESTRICTIONS, EXTRACELLULAR TORTUOSITY, AND EXCHANGE

JOSEF PFEUFFER,*‡ WOLFGANG DREHER,* EVA SYKOVA,† AND DIETER LEIBFRITZ*

*Department of Biology/Chemistry, University of Bremen, 28334 Bremen, Germany; †Department of Neuroscience, Institute of Experimental Medicine AS CR and Second Medical Faculty, Charles University, Prague, Czech Republic; ‡present address: Department of Radiology, Center for MR Research, University of Minnesota, 385 East River Road, Minneapolis, MN 55455, USA

The "concept of restricted intracellular water diffusion at permeable boundaries," which was recently used to model diffusion-weighted ¹H NMR experiments on glioma cells, was applied to measurements on the rat brain *in vivo*. Combined with the "concept of extracellular tortuosity," various physiological states of the brain were simulated. Hereby, a variable intracellular volume fraction, intracellular exchange time, and extracellular tortuosity factor were considered for young, adult, and ischemic rat brains. The model simulated the cytotoxic shift of extracellular water, changes in membrane permeability and tissue morphology, and was able to explain the diffusion time dependence as well as the non-monoexponentiality of the diffusion attenuation curves. Preliminary diffusion time dependent experiments on the healthy rat brain (¹H NMR imaging) agreed well with the theoretical concept. Hereby, the intracellular water signal was separated from extracellular signal contributions by large diffusion weighting. It showed the characteristic of restricted diffusion as well as a signal decay due to the exchange of intracellular water across the plasma membrane. A map of the mean intracellular exchange time for water in living animal brain was determined, and the upper limit in rat brain was evaluated to 15 ms. The presented methods can be applied to correlate local differences in a map of exchange times with tissue morphology and to detect pathological deviations of the exchange time, e.g., during ischemia.   © 1998 Elsevier Science Inc.

Keywords:—Restricted diffusion; Water exchange; Diffusion time dependence; Tortuosity.

INTRODUCTION

Diffusion-weighted nuclear magnetic resonance (NMR) imaging has become a routine clinical utility for detecting brain pathologies, such as early stages of ischemia.[1] Changes in the apparent diffusion coefficient of water (ADC) are used to characterize the status of brain tissue, whereby many experimental and theoretical studies have been made to unravel the underlying mechanisms of the diffusion contrast and its change during a brain infarct.[2–12] The ADC decrease during ischemia is supposed to be mainly caused by the shift of the interstitial water to the intracellular space.[11] The changes in the extracellular volume fraction and the extracellular tortuosity as measured by iontophoresis have not been sufficient to quantify the absolute value of the ADC and its decrease during ischemia.[10,13,14] It has also been proposed that changes in the cell-membrane permeability may cause the observed decrease in the ADC.[15–17]

To explain the complex situation, one has to examine various tissue parameters such as the intra- and extracellular diffusion constants, the exchange time, the extracellular tortuosity, and the intracellular diffusion restriction, and not all parameters can be determined separately. The situation is complicated in tissue because of the cell populations (e.g., neurons and glial cells) and the locally different morphology which introduce microscopic and macroscopic anisotropies with respect to wa-

ter diffusion, i.e. the diffusion coefficients and the tortuosity factors.[8,12,18–22] Therefore, it is difficult to interpret the absolute ADC in different tissue locations as a function of given experimental parameters such as the b value, the diffusion time, the gradient direction, and the tissue state (healthy or pathological).

Non-monoexponential diffusion attenuation curves in immature, adult, and ischemic rat brains have been detected with large diffusion-weighting gradients.[7,23] Extended experimental studies and analytical simulations on perfused cell cultures, dissected nerves and rat brains have been performed to examine the influence of the intracellular restricted water diffusion and of the intra-/extracellular water exchange on the diffusion mediated signal attenuation and its diffusion time dependence.[12,24–27]

In the following, the "concept of restricted intracellular water diffusion at permeable boundaries,"[28,29] which has recently been successfully applied to cell experiments,[27] is adapted to the situation in rat brain tissue and is combined with the "concept of extracellular tortuosity"[30]. Various physiological states are considered for young, adult, and ischemic rats by changing the intracellular volume fraction p_2, the intracellular exchange time τ_2, and the extracellular tortuosity factor λ. The model simulates the cytotoxic shift of extracellular water, alterations in membrane permeability and tissue morphology by different p_2, τ_2, and λ, and is able to explain the diffusion time dependence as well as the non-monoexponentiality of the diffusion attenuation curves.

Preliminary diffusion time dependent ^{1}H NMR imaging experiments are performed on the healthy rat brain *in vivo*, which agree well with the theoretical concept. The intracellular water signal at large diffusion-weighting shows a characteristic of restricted diffusion, as well as a signal decay due to exchange between intra- and extracellular water. To our knowledge, it is the first time that a mean intracellular residence time of water, calculated from the intracellular water signal decay vs. diffusion time, is mapped in living animal brain. It is conceivable that local differences in the map of exchange times will eventually be correlated with the tissue morphology and that changes of the water exchange may alter with pathological disorders.

MODEL

The diffusion attenuation of the water signal measured by the pulsed-field-gradient spin-echo technique has been recently investigated in extended experimental studies and analytical simulations.[27,31,32] The diffusion time dependence of the intracellular water component in perfused glioma cells could be described well by restricted diffusion at permeable boundaries. The cellular

morphology has been characterized by a distribution of propagation lengths, and the mean residence time for intracellular water has been determined to about 50 ms. A combination of the Tanner formula[33] for restricted diffusion in a box and the Kärger equations[34,35] for exchange in a two-compartment system has been used for the analytical model. The signal attenuation $S(\tilde{q}^2, t_D, D_1, D_2, p_2, \tau_2, \bar{a}, \sigma_a)$ has been calculated analytically dependent on the experimental parameters $\tilde{q}^2$ and t_D (q value and diffusion time, see experimental), on the physiological parameters D_1, D_2, p_2, τ_2 (extra-/intracellular diffusion constant, intracellular volume fraction and exchange time), and on a morphological parameter a (box length). A Gaussian distribution of box lengths with mean $\bar{a}$ and width σ_a has been used to account for the complex cellular morphology with regard to cell shape and cell size.

This model will be applied by analogy, but with some modifications, to study changes in the water signal-attenuation curves of brain tissue at different diffusion times and with different physiological parameters during ischemia, i.e. changes of the extra-/intracellular volume ratio and of the exchange time. The standard parameters used for the situation in adult rat brain tissue are $D_1 = 3.0 \cdot 10^{-3}$ mm^2/s, $D_2 = 1.0 \cdot 10^{-3}$ mm^2/s, $p_2 = 0.8$, $\tau_2 = 15$ ms, $\bar{a} = 5$ μm, and $\sigma_a = 10$ μm.

Extracellular Tortuosity

Water diffusion in the interstitial space of the tissue is no longer free, but hindered. The particles have to go longer diffusion pathways around neurons and glial cells, which can be described by a decreased, apparent extracellular diffusion coefficient[8,14,30]

$$D_1^{app} = D_1/\lambda^2 \quad \lambda \ldots \text{tortuosity factor, } \lambda \geq 1, \quad (1)$$

whereas the extracellular diffusion obeys modified Fick's equations, deduced by volume averaging.[30] In this sense, a Gaussian-like propagation can be assumed. Because of anisotropic obstacles, λ has been modelled also anisotropically and depends on the applied-gradient orientation.[12]

Monte Carlo simulations of diffusion in the extracellular space of digitized brain slices have shown[36] that the extracellular volume fraction $\alpha = 1 - p_2$ and the tortuosity factor λ are interconnected by the empirical Archie's law $\lambda = \alpha^{-l}$ found in porous media[37] (note that for the extracellular volume fraction p_1 the more common symbol α is used). The tortuosity exponent in brain tissue has been determined to $l = 0.41$.[36]

Previously, extracellular diffusion has been studied *in vivo* in neonatal and adult rat brains during global ischemia by concentration-time profiles of tetramethylam-

Table 1. Temporal evolution of the tortuosity factor λ and the extracellular volume fraction $\alpha = 1 - p_2$ of (a) young rats (8–12 days old) and (b) adult rats (3 months old), starting from the control before anoxia (first value) and developing after cardiac arrest (successive values) as measured by iontophoresis[10,14]

(a)						
	α	0.27–0.30	0.25	0.15	0.10	0.05
	λ	1.50	1.60	1.80	1.90	2.10
	l	0.31–0.34	0.34	0.31	0.28	0.25
(b)	α	0.20–0.22	0.15	0.10	0.05	0.05*
	λ	1.50	1.70	1.80	2.00	2.10
	l	0.25–0.27	0.28	0.26	0.23	0.25

The values and their time course are dependent on brain region and the age of the animal (compare with references 10, 14); the tortuosity exponent l is calculated by $l = -\ln \lambda / \ln \alpha$; * α remains at 0.05 with ongoing time course, while λ still increases.

monium measured by iontophoresis.[10,13,14] The decrease of α and the corresponding increase of λ has been correlated experimentally with a dynamic decrease of the ADC upon induced ischemia. However, realistic quantitative ADC values could not be deduced considering free extracellular diffusion only. Calculations of the tortuosity exponent l using the data in Ref. 10 (Table 1, Fig. 9) show that Eq. (1) l differs already in healthy neonatal rat brain ($l = 0.31$ in grey and $l = 0.46$ in white matter); Eq. (2) l decreases continuously upon induction of global ischemia; and Eq. (3) l reaches an asymptotic value of ~0.24 (for both grey and white matter) about 30 min after ischemia (compare with Table 1).

Thus, the situation in brain tissue is complicated additionally by the anisotropy and the locally differing microstructure. The exchange of extra- and intracellular water, as described by an uptake parameter in Ref. 14, may affect the dependence of λ, and hereby the dependence of D_1^{app}, on α. The values for the extracellular tortuosity factor λ in our model calculations are taken from Table 1. They can be regarded as a first approximation of the differing experimental data to show up the principal effect of the changing tortuosity. Furthermore, one may keep in mind that Archie's law using a mean tortuosity exponent l might be not sufficient as a starting point of modelling.

Intracellular Restriction and Exchange

Intracellular water diffusion is restricted by the cell membrane resulting in a non-Gaussian propagation characteristic. A diffusion time dependent, apparent intracellular diffusion coefficient:

$$D_2^{app}(t_D) = -\frac{\partial \ln E}{\partial \tilde{q}^2} \cdot \frac{1}{t_D}, \qquad (2)$$

is calculated by the partial derivative of the Tanner formula $E = E(q, a, D_2, t_D)$ for restricted diffusion in a box.[33] The term q value represents here the quantity $\tilde{q}^2 = 4\pi^2 q^2$ which is deduced from $q = \gamma/2\pi \cdot \delta \cdot G$ as

defined in Ref. 38. The Kärger equations[35] for exchange in a two-compartment system are used with D_1^{app} and D_2^{app} (t_D) instead of D_1 and D_2. The signals are weighted and superposed according to normally distributed box lengths with mean $\bar{a}$ and width σ_a. For further details of the analytical model calculation, see Ref. 27. The mean value of the intracellular exchange time $\tau_2 = 15$ ms is used for the healthy adult rat brain which is extracted from the experimental data presented below.

Diffusion Time Dependence

The dependence of the diffusion-weighted signal on the diffusion time is calculated with the standard parameters for the adult rat brain and $t_D = [5 \ldots 500]$ ms (plotted vs. q value in Fig. 1). The ADC is determined from the slope at low q values which declines fast with increasing t_D from $0.79 \cdot 10^{-3}$ mm^2/s to $0.29 \cdot 10^{-3}$
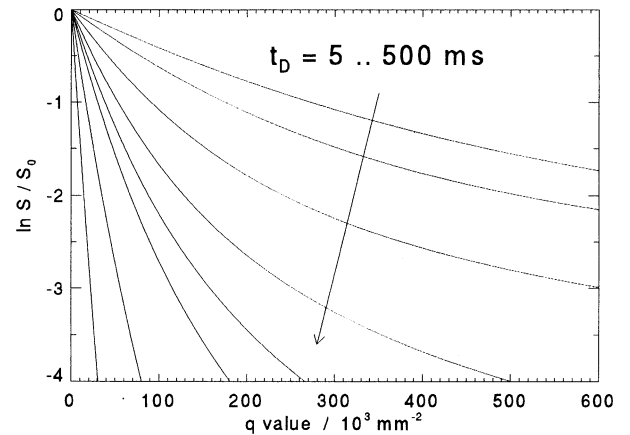

Fig. 1. Model calculation of the diffusion-weighted signal attenuation as a function of the diffusion time $t_D = [5, 10, 25, 50, 75, 100, 200, 500]$ ms, plotted vs. q value. The ADC at low q values is listed in Table 2. The apparent intracellular exchange time is $\tau_2^{app} = 26.2$ ms at $\tilde{q}^2 = 300 \cdot 10^3$ mm^{-2} (see text). Model parameters (adult rat brain tissue): $D_1 = 3.0 \cdot 10^{-3}$ mm^2/s, $D_2 = 1.0 \cdot 10^{-3}$ mm^2/s, $p_2 = 0.8$, $\lambda = 1.5$, $\tau_2 = 15$ ms, $\bar{a} = 5$ μm, $\sigma_a = 10$ μm.

Table 2. Dependence of the ADC on the diffusion time t_D in the rat brain model of Fig. 1

t_D/ms	5	10	25	50	75	100	200	500
ADC/10^{-3} mm²/s	0.79	0.63	0.49	0.41	0.38	0.35	0.31	0.29

The ADC is calculated by log-linear regression of ln S vs. b in the range $b = [0 \ldots 1000]$ s/mm².

mm²/s (see Table 2). As shown by the experiments and simulations on cell cultures,[27] the intracellular water contributes predominantely to the signal at high q values due to the restricted intracellular diffusion. In this case, the slope of ln S vs. q value becomes constant and independent on t_D, which is reached in our model for $q^{-2} > 300 \cdot 10^3$ mm^{-2} (Fig. 1).

An intracellular exchange time of $\tau_2^{app} = 26.2$ ms is determined from the signal decay in Fig. 1 at $\tilde{q}^2 = 300 \cdot 10^3$ mm^{-2} (negative reciprocal slope of ln S vs. t_D). This apparent exchange time exceeds the inserted starting value of $\tau_2 = 15$ ms due to extracellular signal contributions and can be corrected according the formula deduced by Andrasko:[39]

$$\tau_2 \approx \tau_2^{app} - \frac{n}{\tilde{q}^2 D_1^{app} - (\tau_2^{app})^{-1}}. \qquad (3)$$

Wherein the approximation $D_2^{app} \ll D_1^{app}$ is assumed, the complete formula is given in Ref. 39. With $n = p_2/(1 - p_2) = 4$ and $D_1^{app} = 3.0/1.5^2 \cdot 10^{-3}$ mm²/s follows $\tau_2 \approx 14.9$ ms.

Changes of the Diffusion-Attenuation Curves during Ischemia

The dependence of the diffusion-weighted signal attenuation on different physiological conditions is shown in Fig. 2. The intracellular volume fraction p_2 and the intracellular exchange time τ_2 are adapted to simulate ischemia in immature and adult rat brain, and the extracellular tortuosity factor λ is varied with p_2. The detailed parameters and the quantitation evaluation of the attenuation curves are listed in Table 3. The ADC is calculated by log-linear regression in the range of small b values $[0 \ldots 1000]$ s/mm², whereas D_2^{app} and the appertaining intercept p_2^{app} are derived at large b values $[8000 \ldots 10000]$ s/mm².

Increasing p_2 from 70 up to 95% (Fig. 2a) decreases the ADC from 0.73 to $0.40 \cdot 10^{-3}$ mm²/s. A p_2 of 70% corresponds to a healthy immature rat brain, 80% to a healthy adult rat brain. In the course of an anoxic insult, the intracellular volume fraction increases in immature as well as in adult rats to $p_2 = 95\%$. Thus p_2^{app} increases as well as p_2 does. However, the absolute value of p_2^{app} is much lower than p_2. D_2^{app} slightly decreases from 0.1

to $0.09 \cdot 10^{-3}$ mm²/s. Hereby $\tau_2 = 15$ ms is used for the intracellular exchange time. For the ischemic tissue ($p_2 = 95\%$), the simulation fits only if τ_2 is increased to 50 ms (dotted line in Fig. 2a) corresponding to an about threefold decrease in cell membrane permeability. This is estimated to be an upper limit for a physiological permeability change comparing open and blocked water channels in erythrocytes.[39,40]

The ADC shows almost no influence if the intracellular exchange time τ_2 is increased from 15 to 100 ms, while p_2 is kept constant (Fig. 2b). However, the negative slope of the signal attenuation at large b values, i.e. D_2^{app} decreases significantly with increasing τ_2.

The situation of the dynamic tissue swelling in immature rat brain during ischemia is simulated in Fig. 2c (see also Table 1a), while τ_2 is kept constant. A continuous decrease of the ADC as well as a increase of p_2^{app} are observed, D_2^{app} remains nearly constant. If changes of the exchange time τ_2 and of the membrane permeability respectively are considered, D_2^{app} is much more influenced. Analogously dynamic tissue swelling in adult rat brain according to Table 1b is simulated and analysed in Table 3.

For comparison, calculated data based on experimentally determined parameters taken from Ref. 23, are shown in Table 3, too. A decrease in the ADC from 0.83 to $0.36 \cdot 10^{-3}$ mm²/s as well as a decrease of D_2^{app} from 0.22 to $0.11 \cdot 10^{-3}$ mm²/s has been measured which can be well reproduced by the used theoretical model.

EXPERIMENTAL

Diffusion-weighted ^{1}H-NMR images were acquired on a 4.7T/400-mm Biospec system (Bruker, Karlsruhe, Germany), equipped with a 200-mm self-shielded gradient insert, capable of switching 150 mT/m within 450 μs in three directions. Signal excitation was performed using a 94-mm inner diameter saddle-shaped volume coil. The signal was received by an 18-mm surface coil which was actively decoupled from the volume coil. The used diffusion-weighted, phase-cycled ultrafact low-angle RARE imaging sequence has been described previously[41,42] and implemented as follows: image matrix size (32 × 32), SW = 50 kHz, echo time (TE) = 80.5 ms, number of averages = 28, repetition time (TR) = 1.5 s, field of view (FOV) = 32 mm, and slice thickness = 5
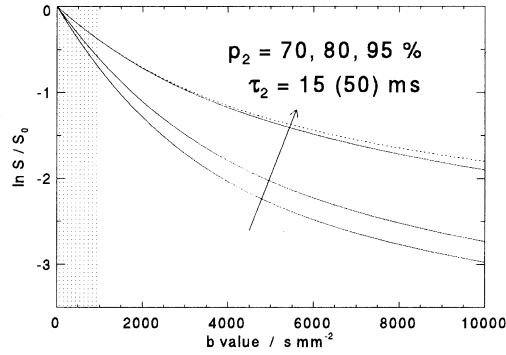
(a)
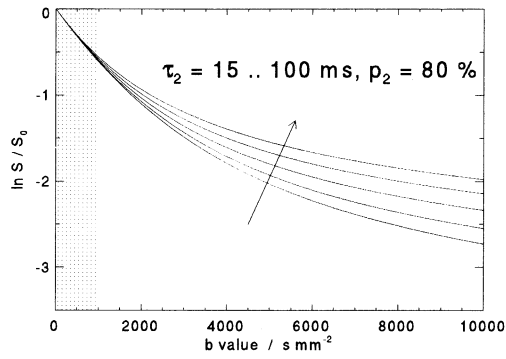
(b)
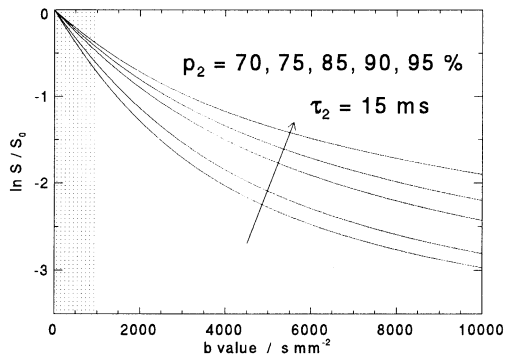
(c)

Fig. 2. Model calculation (as in Fig. 1) of the diffusion-weighted signal attenuation dependent on different physiological conditions (t_D = 16.2 ms). The intracellular volume fraction p_2 and/or the intracellular exchange time τ_2 are varied to simulate ischemia in immature and adult rat brains: a) p_2 and τ_2 variable; b) τ_2 variable and p_2 constant; c) p_2 variable (dynamic tissue swelling in young rats). The extracellular tortuosity factor λ is also changed with varied p_2 according to Table 1. All plot parameters are listed and quantified in Table 3. The dotted curve in (a) refers to τ_2 = 50 ms.

mm. Centered phase-encoding was employed. The refocusing pulses (α = 90°) were Gaussian of 300 μs duration, the scan time for a single shot image including six dummy cycles was 113 ms.

The preparation experiment for the diffusion sensitization was a 90°-τ-180°-τ spin echo sequence with unipolar gradients.[43] The experimental parameter determining the diffusion attenuation were the gradient duration δ, the gradient strength G and the separation Δ of the leading edges of the gradients, which defines the q value $\tilde{q}^2 = (\gamma\delta G)^2$, the diffusion time $t_D = \Delta - \delta/3$, and the b value $b = \tilde{q}^2 t_D$. While keeping the echo time TE constant, T_2 effects were excluded. For a *ct* experiment (constant diffusion time) G = [0 ... 120] mT/m was varied in all three directions by 32 steps, δ = 10 ms and t_D was kept constant. This procedure was performed at the four diffusion times t_D = [17.1, 63.1, 45.1, 31.1] ms (in the order as measured). The result was a four-dimensional image data set $S(x, y, \tilde{q}^2, t_D)$ of size (32 × 32 × 32 × 4) depending on the spatial coordinates, the q value and the diffusion time, sampled within the total acquisition time of 90 min.

$\ln S(\tilde{q}^2, t_D)$ was analyzed for each voxel (x, y) in two ways according to Refs. 27 and 39. The apparent displacement $r^{app} = \sqrt{6m}$ and the apparent intracellular diffusion coefficient $D^{app} = m/t_D$ is calculated from the negative slope m of $\ln S$ vs. $\tilde{q}^2$ at fixed t_D. In contrast, the apparent exchange time τ_2^{app} is calculated from the negative reciprocal slope of $\ln S$ vs t_D at fixed $\tilde{q}^2$. To decrease the error of τ_2^{app} due to the low signal-to-noise ratio at high q values, τ_2^{app} is averaged within the range $\tilde{q}^2$ = [50 ... 304] · 10^3 mm^{-2}.

The preliminary *in vivo* experiments were conducted on two adult Wistar rats. The animals were anesthetized with a mixture of halothane (1.5 vol. %), oxygen (33%), and nitrous oxide (66%). Images were acquired in coronal section through the brain with the slice positioned 4 mm posterior to the frontal pole.

RESULTS AND DISCUSSION

Typical rat data selected from the 4D image set are shown in Fig. 3 (voxel within the striatum). The *ct* data at diffusion times t_D from 17.1 to 63.1 ms are normalized by $S_0 = S(\tilde{q}^2 = 0)$ and plotted vs. q value ($\tilde{q}^2_{max}$ = 304 · 10^3 mm^{-2} corresponds to b_{max} = [5200 ... 19200] s/mm^2 depending on t_D). This has the advantage that the dependence of the signal attenuation S on the experimental parameters $\tilde{q}^2$ and t_D is emphasized. Furthermore, it is possible to distinguish between a free or restricted-diffusion characteristics of the intracellular water signal at high q values. In the case of restricted diffusion, the apparent, intracellular exchange time τ_2^{app} can be evaluated from the signal decay vs. t_D at fixed q value.

Table 3. Quantification of the simulations in Fig. 2 compared with experimental data of Table 1 and Reference 23

Fig. 2a	$p_2/\%$	70	80	95	95	
	λ	1.5	1.5	2.1	2.1	
	τ_2/ms	15	15	15	50	
	ADC	0.73	0.62	0.40	0.40	
	D_2^{app}	0.10	0.10	0.090	0.076	
	$p_2^{app}/\%$	14	18	37	35	
Fig. 2b	$p_2 = 80\%$,	$\lambda = 1.5$	constant			
	τ_2/ms	15	20	30	50	100
	ADC	0.62	0.61	0.60	0.59	0.57
	D_2^{app}	0.10	0.091	0.079	0.071	0.065
	$p_2^{app}/\%$	18	19	21	24	26
Fig. 2c, Table 1a young rats	$p_2/\%$	70	75	85	90	95
	λ	1.5	1.6	1.8	1.9	2.1
	$\tau_2 = 15$ ms	constant				
	ADC	0.73	0.64	0.50	0.44	0.40
	D_2^{app}	0.10	0.10	0.11	0.10	0.090
	$p_2^{app}/\%$	14	17	26	32	37
Table 1b adult rats	$p_2/\%$	80	85	90	95	95
	λ	1.5	1.7	1.8	2.0	2.1
	$\tau_2 = 15$ ms	constant				
	ADC	0.62	0.51	0.46	0.40	0.40
	D_2^{app}	0.10	0.11	0.11	0.091	0.090
	$p_2^{app}/\%$	18	25	30	36	37
Experimental rat data*		immature		adult	global ischemic	
	$p_2/\%$†	57–73		78–80	95	
	ADC	0.83		0.68	0.36	
	$D_2^{app}/\%$	0.22		0.18	0.11	
	$p_2^{app}/\%$	12		19	41	

$[ADC, D] = 10^{-3}$ mm^2/s; ADC is calculated by log-linear regression in the range $b = [0 \ldots 1000]$ s/mm^2, D_2^{app}; p_2^{app} by log-linear regression in the range $b = [8000 \ldots 10000]$ s/mm^2; * calculated data based on experiments of reference 23; † according reference 14.

Intracellular Restriction

The negative slope m of ln S vs. q value (Fig. 3) is analyzed in Table 4. The apparent displacement $r^{app} \sim 3.5~\mu$m becomes constant within the experimental error for $t_D > 30$ ms. The apparent intracellular diffusion coefficient D^{app} decreases rapidly with t_D from 0.19 to $0.032 \cdot 10^{-3}$ mm^2/s. A constant slope of ln S vs. q value (constant r^{app} at different t_D) indicates restricted diffusion of intracellular water which has been shown by experiments and analytical modelling on perfused cell cultures.[27,31,32] In contrast, plots vs. b value are suitable to test the data for free or hindered diffusion.

The measured rat brain data show two different char-

acteristics similar to the data of cell cultures: at low b values the slopes vs. b value are constant indicating free or hindered extracellular diffusion, at high q values ($\tilde{q}^2 > 100 \cdot 10^3$ mm^{-2}) the slopes vs. q value become constant for $t_D > 30$ ms indicating the transition from intracellular free to restricted diffusion with increasing t_D (Fig. 3). The decay of the signal at high q values with constant slope shows additionally that the intracellular water is not totally restricted, but has also the opportunity to exchange across the cell membrane.

Thus the experimental, diffusion time dependent data on rat brain agree well with the concept of a two-compartment model with extracellular hindered diffusion
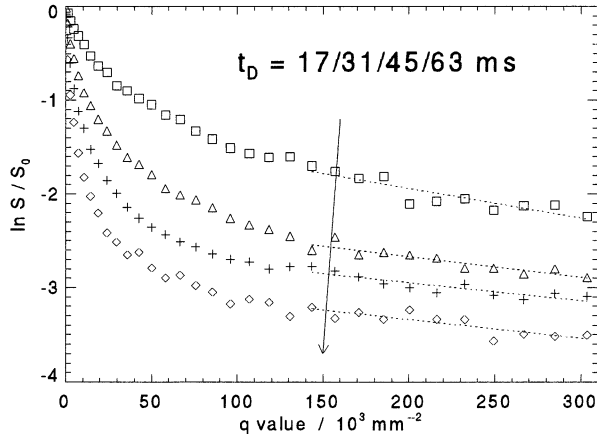
Fig. 3. *ct* experiments at the diffusion times t_D = [17.1 ($\square$), 31.1 ($\triangle$), 45.1 (+), 63.1 ($\diamond$)] ms, measured with the diffusion-weighted U-FLARE sequence. Data are shown from a selected voxel in the striatum. Imaging parameters: 32 × 32 image, field of view = 32 mm, slice thickness = 5 mm, 28 averages, δ = 10 ms, echo time 80.5 ms.

and intracellular restricted diffusion at permeable boundaries and can be described quantitatively. The property of intracellular restricted diffusion legitimizes the separation of intracellular signal contributions at high q values, as the intrinsic intracellular diffusion constant is apparently lowered and extracellular contributions are dephased. The characteristic of restricted diffusion becomes here more evident compared to Ref. 4 where at small b values up to 1500 s/mm^2 intra- and extracellular contributions are still mixed.

Exchange Time

The 4D rat data also can be analyzed to provide information on the exchange of intracellular water. A calculated map of the apparent intracellular exchange times τ_2^{app} is shown in Fig. 4a. Appropriate thresholding yields a reasonable outline of the two rat brain halves. An exchange time cross section, indicated by the two arrows in the map, is plotted in Fig. 4b with the accompanying standard deviations. The larger values of τ_2^{app} in the striatum of about 35 ms suggest that this probably reflects the local morphological differences in brain tissue.

This resembles the behaviour of the diffusion tensor anisotropy which is caused by the anisotropic tissue structure. Although the exchange time seem to indicate a difference between left and right hemisphere, the complementary τ_2^{app} are the same within the experimental error. The histogram of the intensities of the exchange time map is shown in Fig. 4c. A fitted Gaussian distribution yields τ_2^{app} = (26.5 ± 5.4) and (24.0 ± 4.5) ms for the two measured rats.

The intrinsic intracellular exchange time τ_2 is calculated from Eq. 3 to τ_2 = 15.4 and 12.8 ms (inserting n = 4, $\tilde{q}^2$ = 300 · 10^3 mm^{-2}, D_1^{app} = 3.0/1.5^2 · 10^{-3} mm^2/s). Another aspect, discussed more in detail in Ref. 27, has to be considered. A particle leaving one cell may diffuse into a neighbor cell via the small extracellular space. Thus τ_2, being a mean residence time at the intracellular site, overestimates the residence time of water in single cells.

The performed *ct* experiments yielding a 4D image data set is, of course, not the optimum acquisition method if one is interested in mapping the intracellular exchange time. The *ct* method has been chosen here to make clear that the concept of intracellular restriction with exchange holds for brain tissue as well as for cell cultures. The next step is to perform immediately *cg* (constant gradient strength) imaging experiments at high q values keeping G constant and varying Δ, *i.e.*, the diffusion time. This will reduce measurement time and will allow to determine τ_2^{app} and τ_2 much more accurately at a fixed q value. Probably local differences in the map of exchange times may be correlated with the tissue morphology. In this context anisotropic tortuosity factors in relation to the anisotropic water diffusion properties will have to be also considered. Furthermore, changes of τ_2^{app} are to be expected during the time course of ischemia as both, the experimental and the simulated data in Table 3 (immature, adult, and ischemic rats) suggest.

The modelling results propose that changes in τ_2 have negligible influence on the ADC at low b values, but a sizeable effect on D_2^{app} at larger b values, where mainly intracellular water signal can be selected by the high diffusion-weighting. It will be necessary to examine whether experimentally observable changes in τ_2^{app} are solely caused by the shift of extra- to intracellular water,

Table 4. Analysis of the slope m of ln S vs. q value (Fig. 3) with the calculation of the apparent displacement r^{app} and the apparent diffusion coefficient D^{app}

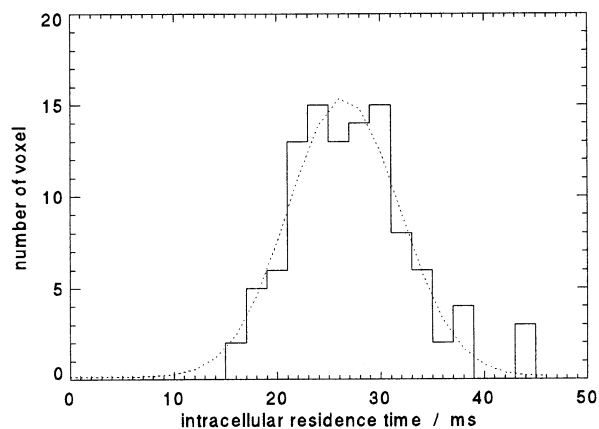| t_D/ms	17.1	31.1	45.1	63.1
r^{app}/μm	4.4 ± 0.4	3.7 ± 0.3	3.4 ± 0.3	3.5 ± 0.4
D^{app}/10^{-3} mm^2/s	0.19 ± 0.03	0.072 ± 0.010	0.043 ± 0.007	0.032 ± 0.006

$r^{app} = \sqrt{6m}$, $D^{app} = m/t_D$; the negative slope m of ln S vs. $\tilde{q}^2$ is calculated by log-linear regression in the range $\tilde{q}^2$ = [144 . . . 304] · 10^3 mm^{-2}.
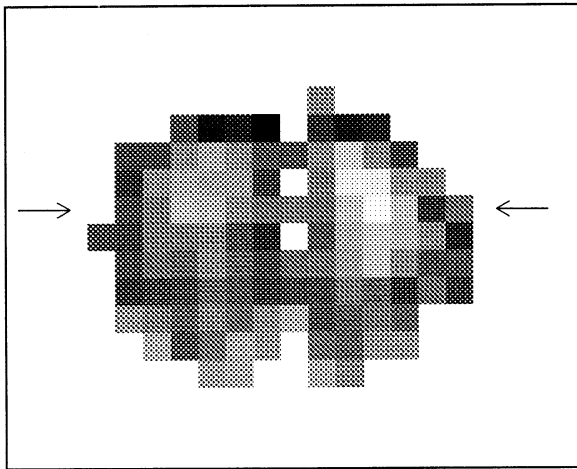
(a)
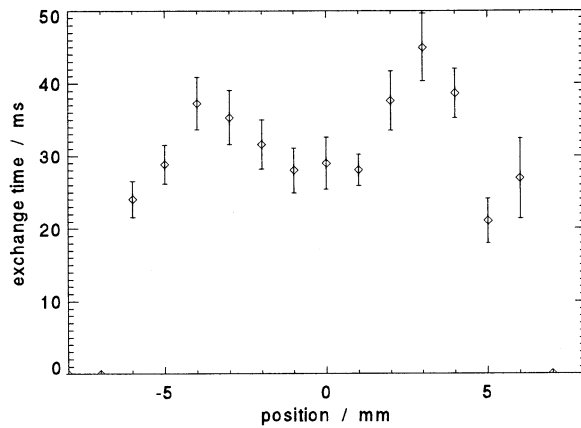
(b)

(c)

Fig. 4. Mean apparent intracellular residence times τ_2^{app} in the adult, healthy rat brain: a) map of exchange times, calculated from the signal attenuation vs. diffusion time at large q values; b) selected profile of exchange times (as indicated by arrows in a); c) histogram of exchange times of the total brain. A Gaussian fit (dotted line) yields $\tau_2^{app} = (26.5 \pm 5.4)$ ms.

or by a decrease in membrane permeability. The latter could be explained by the mechanism of a stretch-activated blocking of the water channels,[44–47] which would increase τ_2^{app} significantly. The identification and location of water channels in brain and glial cells has been reported, whereas their functionality under healthy and pathophysiological conditions, e.g., regulation of brain edema, is still disputed.[17,48–51]

CONCLUSIONS

The diffusion behaviour of water in rat brain tissue can be modelled analytically by restricted intracellular diffusion at permeable boundaries combined with extracellular tortuosity. The diffusion time dependent and non-monoexponential diffusion attenuation curves are influenced by changes of the volume fraction, the exchange time, and the tortuosity factor. Intracellular water signal can be separated from extracellular signal contributions with large diffusion-weighting. A map of the mean intracellular residence time for water in rat brain is determined from the signal decay vs. diffusion time by diffusion-weighted ^{1}H NMR imaging experiments *in vivo*. The upper limit of the intrinsic intracellular exchange time is estimated to 15 ms. A further time and spatially resolved monitoring of the water exchange time during ischemia may elucidate the interacting physiological mechanisms.

REFERENCES

1. Moseley, M.E.; Butts, K.; Yenari, M.A.; Marks, M.; de Crespigny, A. Clinical aspects of DWI. NMR Biomed. 8:387–396; 1995.
2. Benveniste, H.; Heldlun, L.W.; Johnson, G.A. Mechanism of detection of acute cerebral ischemia in rats by diffusion weighted magnetic resonance microscopy. Stroke 23:746–754; 1992.
3. Latour, L.L.; Svoboda, K.; Mitra, P.P.; Sotak, C.H. Time-dependent diffusion of water in a biological model system. Proc. Natl. Acad. Sci. USA 91:1229–1233; 1994.
4. Norris, D.G.; Niendorf, T.; Leibfritz, D. Healthy and infarcted brain tissues studied at short diffusion times: the

origin of apparent restriction and the reduction in apparent diffusion coefficient. NMR Biomed. 7:304–310; 1994.

5. Szafer, A.; Zhong, J.; Gore, J.C. Theoretical model for water diffusion in tissues. Magn. Reson. Med. 33:697–712; 1995.

6. Szafer, A.; Zhong, J.; Anderson, A.W.; Gore, J.C. Diffusion-weighted imaging in tissues: Theoretical models. NMR Biomed. 8:289–296; 1995.

7. Helmer, K.G.; Dardzinski, B.J.; Sotak, C.H. The application of porous-media theory to the investigation of time-dependent diffusion in *in vivo* systems. NMR Biomed. 8:297–306; 1995.

8. Bihan, D.L. Molecular diffusion, tissue microdynamics and microstructure. NMR Biomed. 8:375–386; 1995.

9. Hoehn-Berlage, M.; Eis, M.; Back, T.; K.,K.; Yamashita, K. Changes of relaxation times (T_1, T_2) and apparent diffusion coefficient after permanent middle cerebral artery occlusion in the rat: Temporal evolution, regional extent, and comparison with histology. Magn. Reson. Med. 34:824–834; 1995.

10. van der Toorn, A.; Sykova, E.; Dijkhuizen, R.M.; Vorisek, I.; Vargova, L.; Skobisova, E.; van Lookeren Campagne, M.; Reese, T.; Nicolay, K. Dynamic changes in water ADC, energy metabolism, extracellular space volume, and tortuosity in neonatal rat brain during global ischemia. Magn. Reson. Med. 36:52–60; 1996.

11. Anderson, A.W.; Zhong, J.; Petroff, O.A.C.; Szafer, A.; Ransom, B.R.; Prichard, J.W.; Gore, J.C. Effects of osmotically driven cell volume changes on diffusion-weighted imaging of the rat optic nerve. Magn. Reson. Med. 35:162–167; 1996.

12. Stanisz, G.J.; Szafer, A.; Wright, G.A.; Henkelman, R.M. An analytical model of restricted diffusion in bovine optic nerve. Magn. Reson. Med. 37:103–111; 1997.

13. Lehmenkühler, A.; Sykova, E.; Svoboda, J.; Zilles, K.; Nicholson, C. Extracellular space parameters in the rat neocortex and subcortical white matter during postnatal development determined by diffusion analysis. Neuroscience 55:339–351; 1993.

14. Vorisek, I.; Sykova, E. Ischemia-induced changes in the extracellular space diffusion parameters, K^+, and pH in the developing rat cortex and corpus callosum. J. Cereb. Blood Flow Metab. 17:191–203; 1997.

15. Helpern, J.A.; Ordidge, R.J.; Knight, R.A. The effect of cell membrane water permeability on the apparent diffusion coefficient of water. In: Book of abstracts: 11th Annual Meeting of the Society of Magnetic Resonance Medicine, Vol. 1. Berlin: SMRM; 1992:1201.

16. Waldeck, A.R.; Nouri-Sorkhabi, M.H.; Sullivan, D.R.; Kuchel, P.W. Effects of cholesterol on transmembrane water diffusion in human erythrocytes measured using pulsed field gradient NMR. Biophys. Chem. 55:197–208; 1995.

17. Pfeuffer, J.; Bröer, S.; Bröer, A.; Flögel, U.; Leibfritz, D. Water channels in glial cells detected by diffusion-weighted ^{1}H NMR spectroscopy. In: Book of Abstracts: 5th Scientific Meeting of the Society of Magnetic Resonance Medicine, Vol. 1. Vancouver: ISMRM; 1997:508.

18. Cleveland, G.G.; Chang, D.C.; Hazlewood, C.F.; Rorschach, H.E. Nuclear magnetic resonance measurement of skeletal muscle: anisotrophy of the diffusion coefficient of the intracellular water. Biophys. J. 16:1043–1053; 1976.

19. Beaulieu, C.; Allen, P.S. Determinants of anisotropic water diffusion in nerves. Magn. Reson. Med. 31:394–400; 1994.

20. Henkelman, R.M.; Stanisz, G.J.; Kim, J.K.; Bronskill, M.J. Anisotropy of NMR properties of tissues. Magn. Reson. Med. 32:592–601; 1994.

21. Basser, P.J. Inferring microstructural features and the physiological state of tissues from diffusion-weighted images. NMR Biomed. 8:333–344; 1995.

22. Pierpaoli, C.; Basser, P.J. Toward a quantitative assessment of diffusion anisotropy. Magn. Reson. Med. 36:893–906; 1996.

23. Niendorf, T.; Dijkhuizen, R.M.; Norris, D.G.; van Lookeren Campagne, M.; Nicolay, K. Biexponential diffusion attenuation in various states of brain tissue: Implications for diffusion-weighted imaging. Magn. Reson. Med. 36:847–857; 1996.

24. Pilatus, U.; Shim, H.; Artemov, D.; Davis, D.; van Zijl, P.C.M.; Glickson, J. Intracellular volume and apparent diffusion constants of perfused cancer cell cultures as measured by NMR. Magn. Reson. Med. 37:825–832; 1997.

25. Assaf, Y.; Cohen, Y. Diffusion of water and metabolites in brain tissue as a function of the diffusion time. In: Book of abstracts: 5th Scientific Meeting of the Society of Magnetic Resonanic Medicine Vol. 2. Vancouver: ISMRM; 1997:1254.

26. Seo, Y.; Morita, Y.; Kusaka, Y.; Steward, M.C.; Murakami, M. Diffusion of water in rat sciatic nerve measured by ^{1}H pulsed field gradient NMR: Compartmentation and anisotropy. Jpn. J. Physiol. 46:163–169; 1996.

27. Pfeuffer, J.; Flögel, U.; Dreher, W.; Leibfritz, D. Restricted diffusion and exchange of intracellular water: Theoretical modelling and diffusion time dependence of ^{1}H NMR measurements on perfused glial cells. NMR Biomed. 11:19–31, 1998.

28. Tanner, J.E. Transient diffusion in a system partitioned by permeable barriers. Application to NMR measurement. J. Chem. Phys. 69:1748–1754; 1978.

29. von Meerwall, E.; Ferguson, R.D. Interpreting pulsed-gradient spin-echo diffusion experiments with permeable membranes. J. Chem. Phys. 74:6956–6959; 1981.

30. Nicholson, C.; Phillips, J.M. Ion diffusion modified by tortuosity and volume fraction in the extracellular microenvironment of the rat cerebellum. J. Physiol. 321:225–257; 1981.

31. Pfeuffer, J. Beschränkte Diffusion und Austausch von Wasser in Zellkulturen und im Gehirn: Theoretische Modelle und ^{1}H-NMR-Messungen. Dissertation Universitat Bremen 1996, Germany; Shaker Verlag, Aachen, 1997.

32. Pfeuffer, J.; Flögel, U.; Leibfritz, D. Monitoring of cell volume and water exchange time in perfused cells by diffusion-weighted ^{1}H NMR spectroscopy. NMR Biomed. 11:11–18, 1998.

33. Tanner, J.E.; Stejskal, E.O. Restricted self-diffusion of protons in colloidal systems by the pulsed-gradient, spin-echo method. J. Chem. Phys. 49:1768–1777; 1968.

34. Kärger, J. Zur Bestimmung der Diffusion in einem Zwei-bereichsystem mit Hilfe von gepulsten Feldgradienten. Ann. Physik 7. Folge 24:1–4; 1969.

35. Kärger, J.; Pfeifer, H.; Heink, W. Principles and application of self-diffusion measurements by nuclear magnetic resonance. Adv. Magn. Res. 12:1–89; 1988.

36. Lipinski, H.-G. Monte Carlo simulation of extracellular diffusion in brain tissues. Phys. Med. Biol. 35:441–447; 1990.

37. Archie, G.E. The electrical resistivity log as an aid in determining some reservoir characteristics. Trans. Am. Inst. Miner. Metall. Eng. 146:54–62; 1942.

38. Callaghan, P.T. Principles of nuclear magnetic resonance microscopy. Clarendon Press: Oxford: 1991.

39. Andrasko, J. Water diffusion permeability of human erythrocytes studied by a pulsed gradient NMR technique. Biochim. Biophys. Acta 428:304–311; 1976.

40. Benga, G.; Pop, V.I.; Popescu, O.; Borza, V. On measuring the diffusional water permeability of human red blood cells and ghosts by nuclear magnetic resonance. J. Biochem. Biophys. Meth. 21:87–102; 1990.

41. Norris, D.G.; Börnert, P.; Reese, T.; Leibfritz, D. On the application of ultra-fast RARE experiments. Magn. Reson. Med. 27:142–164; 1992.

42. Norris, D.G.; Börnert, P. Coherence and interference in ultrafast RARE experiments. J. Magn. Res. A 105:123–127; 1993.

43. Stejskal, E.O.; Tanner, J.E. Spin diffusion measurements: Spin echoes in the presence of a time-dependent field gradient. J. Chem. Phys. 42:288–292; 1965.

44. Agre, P.; Preston, G.M.; Smith, B.L.; Jung, J.S.; Raina, S.; Moon, C.; Guggino, W.B.; Nielsen, S. Aquaporin CHIP: The archetypal molecular water channel. Am. J. Physiol. 265:F463–F476; 1993.

45. van Os, C.H.; Deen, P.M.T.; Dempster, J.A. Aquaporins: Water selective channels in biological membranes. Molecular structure and tissue distribution. Biochim. Biophys. Acta 1197:291–309; 1994.

46. Knepper, M.A. The aquaporin family of molecular water channels. Proc. Natl. Acad. Sci. USA 91:6255–6258; 1994.

47. Benga, G. Water channels in membranes. Cell Biol. Int. 18:829–833; 1994.

48. Jung, J.S.; Bhat, R.V.; Preston, G.M.; Guggino, W.B.; Baraban, J.M.; Agre, P. Molecular characterization of an aquaporin cDNA from brain: Candidate osmoreceptor and regulator of water balance. Proc. Natl. Acad. Sci. USA 91:13052–13056; 1994.

49. Nielsen, S.; Nagelhus, E.A.; Amiry-Moghaddam, M.; Bourque, C.; Agre, P.; Ottersen, O.P. Specialized membrane domains for water transport in glial cells: high-resolution immunogold cytochemistry of aquaporin-4 in rat brain. J. Neurosci. 17:171–180; 1997.

50. Agre, P.; Brown, D.; Nielsen, S. Aquaporin water channels: Unanswered questions and unresolved controversies. Curr. Opin. Cell Biol. 7:472–483; 1995.

51. King, L.S.; Agre, P. Pathophysiology of the aquaporin water channels. Annu. Rev. Physiol. 58:619–648; 1996.